JMEPEG (2022) 31:3151–3158
https://doi.org/10.1007/s11665-021-06428-2

1059-9495/$19.00

Effect of V Content on Phase Formation and Mechanical Properties of the CoFeNiMnV*x* High-Entropy Alloys

Man Zhu, Mao Zhang, Lijuan Yao, ZiQi Jie, Yongqin Liu, Kun Li, and Zengyun Jian

Submitted: 5 February 2021 / Revised: 22 September 2021 / Accepted: 29 October 2021 / Published online: 15 November 2021

The sigma phase (σ phase) helps to enhance the mechanical properties of high-entropy alloys (HEAs). In this study, several CoFeNiMnV$_x$ (x = 0.25, 0.50, 0.75, 1.00, 1.25, and 1.50) HEAs were synthesized using vacuum arc melting to improve the strength of face-centered cubic (FCC)-type CoFeNiMn HEAs. Vanadium (V)'s influence on the microstructure evolution and compressive properties is investigated. Further, only a single-phase FCC solid solution is observed for alloys with $x \leq 1.00$. In contrast, a mixture of FCC solid solution and intermetallic σ phase is observed for alloys with $x > 1.00$. The FCC phase lattice constant first increases and then decreases slightly with an increase in V content. Adding V improves the strength and microhardness of FCC-type CoFeNiMn HEAs but decreases their ductility. As V content increases, the yield strength significantly increases from 223 to 1545 MPa, whereas the fracture strain decreases from >55% (no fracture) to about 9.5%. Increasing V content also results in an increase in microhardness from 213 to 716 HV.

Keywords high-entropy alloy, microstructure, mechanical property, sigma phase

1. Introduction

High-entropy alloys (HEAs), first proposed by Yeh et al. (Ref 1, 2), are a new type of material defined as alloys consisting of at least five principal elements with each principal element's concentration ranging from 5–35 at.%. HEAs have attracted increasing attention in the last decade due to their excellent mechanical properties, good corrosion resistance, and oxidation resistance. They are currently a hot research frontier in the metallic material field and promising materials for industrial applications (Ref 3–13). Therefore, developing new types of HEAs with outstanding mechanical properties is of theoretical significance and practical value.

HEAs form simple solid-solution structures with body-centered cubic (BCC) or face-centered cubic (FCC) structures due to the effect of high mixing entropy and the formation of intermetallic phases is restricted. However, an experimental observation demonstrated that introducing alloying elements, such as V, Ti, Mn, Mo, and Cr, into the HEAs, forms complex multiphase structures (i.e., Laves or sigma (σ) phase) in the microstructure (Ref 14–17). Thus, the high mixing entropy is not sufficient to prevent the formation of the intermetallic phases. Stepanov et al. (Ref 18) investigated the influence of V addition on the microstructure and mechanical properties of CoCrFeMnNiV$_x$ HEAs and highlighted the formation of σ phase in the CoCrFeMnNiV$_x$ alloy microstructure with $x \geq 0.5$, and an increasing amount of σ phase significantly increases the yield strength and microhardness. Qin et al. (Ref 19) reported that Nb and Ti addition forms Laves and σ phases, which improves the strength of FCC-type CoCrFeMnNi HEAs. They discovered that the yield strength increases from 202 to 1322 MPa with an increase in Ti content from 0 to 12 at.%, for the $(CoCrFeMnNi)_{100-x}Ti_x$ HEAs. Chen et al. (Ref 20) experimentally investigated $Al_{0.5}CoCrCuFeNiV_x$ HEAs and indicated that the hardness increases with the V content ranging from 0.4 to 1.0, and needle-shaped σ phase forms in BCC spinodal structure for alloys with V contents at x = 0.6–1.0. Yurchenko et al. (Ref 21) investigated the effect of Al content on the structure and mechanical properties of $Al_xCrNbTiVZr$ HEAs. They discovered that Al addition alters their structure from a BCC with C15 Laves phases to BCC with two C14 Laves phases, and an increasing Al content enhances the alloy's high-temperature yield strength. Single-phase FCC-type CoFeNiMn HEAs exhibited outstanding ductility and magnetic properties (Ref 22). The V element promotes the enhancement of strength in HEAs. Thus, it is reasonable to develop novel CoFeNiMnV HEAs due to the strengthening effect of V addition. However, the effects of V addition on the microstructure formation and mechanical properties of FCC-CoFeNiMn HEAs remain unknown.

In this study, the equiatomic CoFeNiMn HEAs with single-phase FCC solid solution were selected as the matrix. The effects of V element on the phase evolution, microstructure, and mechanical properties of the CoFeNiMnV$_x$ (x = 0.25, 0.50, 0.75, 1.00, 1.25, and 1.50) HEAs were studied in detail. The formation of an intermetallic σ phase was revealed. In addition, the relationship between mechanical properties and microstructure was investigated.

2. Experimental Details

Alloy ingots with nominal composition of CoFeNiMnV$_x$ (x = 0.25, 0.50, 0.75, 1.00, 1.25, and 1.50 in molar fraction, denoted as $V_{0.25}$, $V_{0.50}$, $V_{0.75}$, $V_{1.00}$, $V_{1.25}$, and $V_{1.50}$,

Man Zhu, Mao Zhang, Lijuan Yao, ZiQi Jie, Yongqin Liu, Kun Li, and **Zengyun Jian**, School of Materials Science and Chemical Engineering, Xi'an Technological University, Xi'an, Shaanxi 710021, People's Republic of China. Contact e-mail: zhuman0428@126.com.

respectively) alloys were arc-melted. Pure metals with > 99.9 wt% purity were used as raw materials. The alloys were repeatedly melted six times with the aid of electromagnetic stirring to ensure compositional homogeneity.

The specimens were cut using a wire-electrode cutting machine and were further polished and etched for metallurgical observation. X-ray diffractometry (XRD; Bruker D8 Advance) with Cu Kα radiation was used to identify their phase constitution, which was examined using the diffraction angle (2θ) from 20 to 100° at a scanning rate of $4°\cdot min^{-1}$. The microstructure of these alloys was characterized using scanning electron microscopy (SEM; FEI Quanta 400F) equipped with energy dispersive spectrometry (EDS; Oxford Inca 350). The compression tests were conducted on an electronic universal testing machine (Instron 5985) at a strain rate of 2×10^{-4} s^{-1} at room temperature. The samples with a 5 mm × 5 mm × 10 mm dimension were prepared for compression test. Vickers microhardness, HV, was measured on the cross-sectional surfaces using a 402MVD Vickers microhardness tester under 100 g load applied for 15 s. Each Vickers microhardness value was the average value of 15 random points.

3. Results and Discussion

3.1 XRD Analysis

Figure 1 shows the XRD patterns obtained from the $CoFeNiMnV_x$ (x = 0.25, 0.50, 0.75, 1.00, 1.25, and 1.50) HEAs. Figure 1(a) shows that only pattern-related FCC phase structure was detectable for the alloys with x ranging from 0.25 to 1.00. The σ phase precipitates in the microstructure of alloys with $x > 1.00$. The relative intensity for the σ phase was enhanced as the V content increased to $x = 1.50$, suggesting a further increase in the fraction of the σ phase. These results indicated that V addition promoted the phase transition from FCC to σ in the $CoFeNiMnV_x$ HEAs. Figure 1(b) displays the

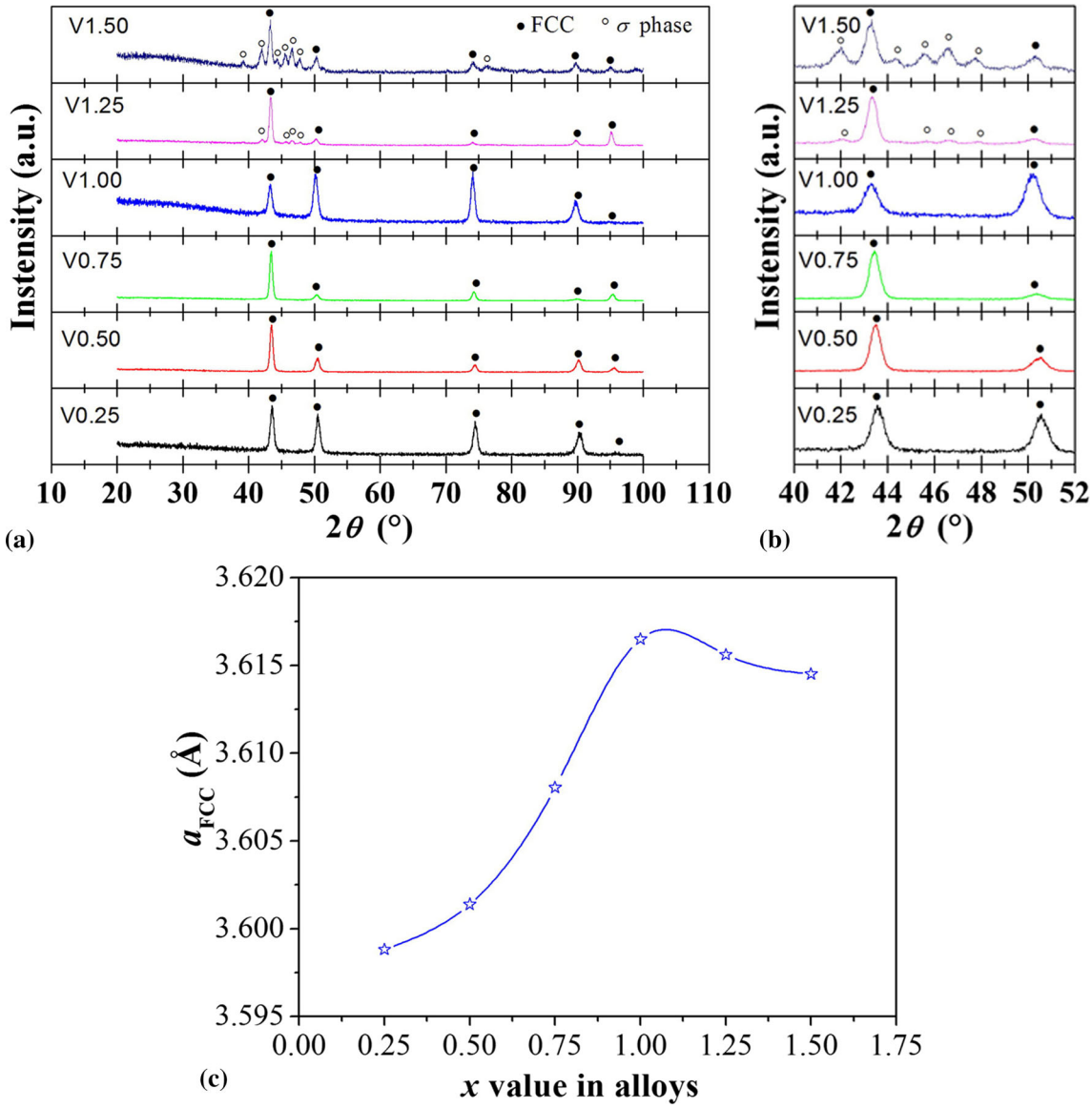

Fig. 1 XRD patterns (a), the enlarged image of the diffraction peaks in the range of 40–52° (b), and lattice constant for the FCC phase in the $CoFeNiMnV_x$ HEAs (c)

enlarged image showing the diffraction peaks ranging from 40 to 52°. The lattice constant (a_{FCC}) for the FCC phase was calculated using Bragg's law "$2d\sin\theta = n\lambda$." Figure 1(c) shows that the a_{FCC} increased steadily for alloys with $x \leq 1.00$, whereas it decreased for alloys with $x > 1.00$. The dissolution of solute atoms in the matrix enhanced the lattice constant of the alloys. However, as the x value increases by 1.00, σ phase precipitation releases the lattice distortion energy, decreasing the lattice constant (Ref 23, 24).

3.2 Microstructure Characterization of the CoFeNiMnV$_x$ Alloys

SEM under back-scattered electron (BSE) mode was used for microstructural characterization, and the local chemical composition was analyzed using EDS. Figure 2(a–f) illustrates the typical microstructure of the CoFeNiMnV$_x$ (x = 0.25, 0.50, 0.75, 1.00, 1.25, and 1.50) HEAs. Table 1 presents the composition of various phases identified in the CoFeNiMnV$_x$ HEAs using EDS. The $V_{0.25}$ alloys exhibited a dendritic structure (Fig. 2a). The dendrite regions (gray ones) were slightly enriched with Co, Fe, and V. They contained about 21.72–22.40% of both Mn and Ni, identified as FCC solid solution, and their chemical compositions corresponding to the alloy nominal composition. However, the interdendritic regions (dark black ones) were enriched with Mn (38.70%) and Ni (26.66%). They contained about 16.16% Co, 14.28% Fe, and 4.20% V. Thus, the interdendritic region was an (Mn, Ni)-rich phase. Figure 2(b–d) shows that the V content in the dendrite and interdendritic regions increased correspondingly for the $V_{0.50}$, $V_{0.75}$, $V_{1.00}$, and $V_{1.25}$ alloys. The precipitation of σ phase (white ones) was observed, and the amount of FCC phase was reduced in the $V_{1.25}$ alloys Fig. 2(e The microstructure revealed the coexistence of the FCC, (Mn, Ni)-rich, and σ phases. Figure 2(f) exhibits the microstructure of the $V_{1.50}$ alloys. The fraction of the FCC phase decreased, whereas that of the σ phase significantly increased, which was consistent with the XRD analysis. Thus, it can be concluded that V addition in the CoFeNiMn HEAs promoted the formation of σ phase .

The chemical compositions of the FCC, (Mn, Ni)-rich, and σ phases vary with V content in the CoFeNiMnV$_x$ HEAs. By increasing the V content, the variation of Co, Fe, Ni, Mn, and V contents within the FCC phase correlated with the average contents of these elements in the CoFeNiMnV$_x$ HEAs. The Co, Fe, and V contents in the (Mn, Ni)-rich phase were lower than the average compositions of these elements in the alloy, whereas the Mn and Ni contents in the (Mn, Ni)-rich phase were higher than the average compositions of these elements in the alloy. EDS analysis of the σ-phase containing alloys revealed that the total atomic concentration of V within the σ phase reached about 28%. In addition, the compositions of the σ phase in the $V_{1.25}$ and $V_{1.50}$ HEAs were almost the same.

3.3 Phase Formation in the CoFeNiMnV$_x$ HEAs

The evolved phases in the CoFeNiMnV$_x$ HEAs, such as FCC and σ phase, were relatively simple. Increasing V content resulted in the precipitation of σ phase. Several criteria were used to predict the phase formation in the HEAs (Ref 25–28). The atomic size difference (δ) is expressed as (Ref 27, 28),

$$\delta = 100\sqrt{\sum_{n=1}^{n} c_i\left(1 - r_i \Big/ \sum_{n=1}^{n} c_i r_i\right)^2} \quad \text{(Eq 1)}$$

where c_i and r_i are the mole fraction and atomic radius of the ith element, respectively.

Further, the high mixing enthalpy promoted the formation of a simple solid-solution phase in the HEAs. Moreover, Yang and Zhang (Ref 25), proposed a parameter, Ω, to reveal the synergistic effect of the mixing entropy (ΔS_{mix}) and enthalpy of mixing (ΔH_{mix}). The expressions of ΔS_{mix}, ΔH_{mix}, and Ω are given as,

$$\Delta S_{mix} = -R\sum_{i=1}^{n} c_i \ln c_i \quad \text{(Eq 2)}$$

$$\Delta H_{mix} = \sum_{i=1, i\neq j}^{n} \left(4\Delta H_{mix}^{ij}\right) c_i c_j \quad \text{(Eq 3)}$$

$$\Omega = \frac{T_m \Delta S_{mix}}{|\Delta H_{mix}|}, T_m = \sum_{i=1}^{n} c_i (T_m)_i, \quad \text{(Eq 4)}$$

where c_i and c_j represent the mole fraction of the ith and jth element, respectively, ΔH_{mix}^{ij} is the enthalpy of mixing for the i–j binary alloy system, T_m is the average melting temperature, $(T_m)_i$ is the melting temperature of the ith element, , and R is an ideal gas constant.

Valence electron concentration (VEC) and Allen electronegativity ($\Delta\chi_A$) are two key physical parameters in estimating phase formation in HEAs (Ref 21, 26, 27). VEC and $\Delta\chi_A$ are expressed as follows:

$$\text{VEC} = \sum_{i=1}^{n} c_i (\text{VEC})_i \quad \text{(Eq 5)}$$

$$\Delta\chi_A = \sqrt{\sum_{i=1}^{n} c_i \left(1 - \chi_i^A - \sum_{i=1}^{n} c_i \chi_i^A\right)^2} \quad \text{(Eq 6)}$$

where c_i is the mole fraction of the ith element, $(\text{VEC})_i$ represents VEC for the ith element, and χ_i^A is the Allen electronegativity of the ith element.

Table 2 lists the physical parameters of the main constituent elements of the CoFeNiMnV$_x$ HEAs (Ref 27, 29). The mixing enthalpies between the major constituent elements are obtained from reference (Ref 30), and their values are summarized in Table 3.

Using Eq 1–6, the calculated values of ΔH_{mix}, ΔS_{mix}, Ω, VEC, δ, and $\Delta\chi_A$ of the CoFeNiMnV$_x$ HEAs are listed in Table 4. The ΔH_{mix} becomes more negative upon V addition in the CoFeNiMnV$_x$ HEAs. The ΔH_{mix} decreases from − 5.76 to − 10.05 kJ·mol^{-1} as V content increases from x = 0.25 to x = 1.25. However, the ΔS_{mix} first increased and then decreased slightly with an increase in V content, and it reached a maximum value of 13.38 J·mol^{-1}·K^{-1} for equiatomic CoFeNiMnV HEAs. Meanwhile, the parameter, Ω, decreased steadily from 3.83 to 2.42, with increasing V content. The value of $T_m\Delta S_{mix}$ is the driving force to form solid–solution, whereas $|\Delta H_{mix}|$ describes the solid-solution formation resistance. Large ΔS_{mix} indicates that the degree of confusion in the

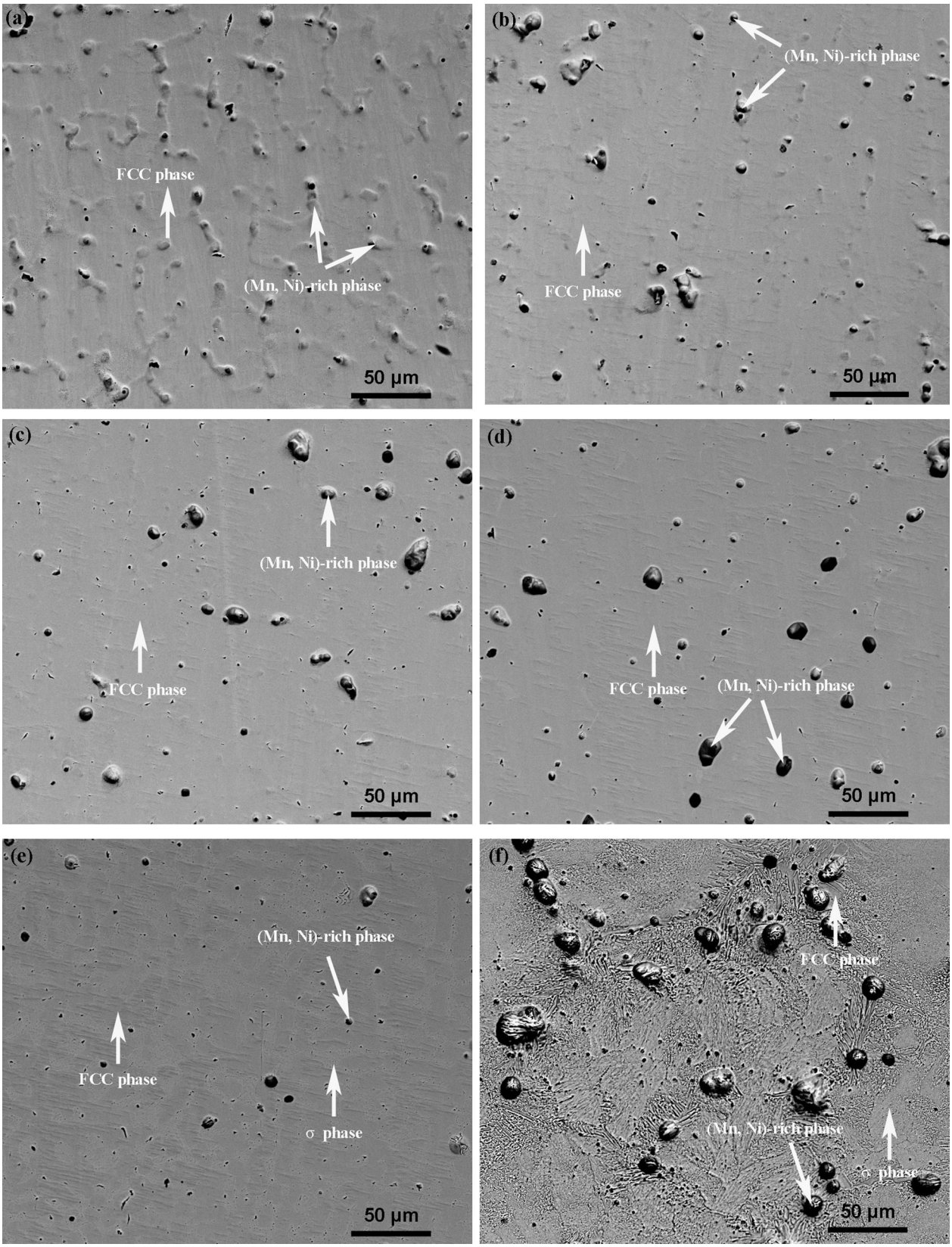

Fig. 2 BSE/SEM images showing the microstructure of the $CoFeNiMnV_x$ HEAs. (a) x = 0.25, (b) x = 0.50, (c) x = 0.75, (d) x = 1.00, (e) x = 1.25, and (f) x = 1.50

alloy system is increased, allowing solid solution to form easily and more stable than intermetallic compounds. The decreased Ω demonstrates that ΔS_{mix} negatively affects the solid-solution formation compared with ΔH_{mix}. The lower the enthalpy of mixing is, the higher the chemical reaction probability. Large negative ΔH_{mix} is the driving force for (FCC + σ) dual-phase

microstructure formation (Ref 29). The decreased Ω hindered the FCC phase formation and promoted the σ phase formation. The V element exhibits stronger negative ΔH_{mix} with the main constitution elements (i.e., V–Co: −14 kJ·mol^{-1}, V–Fe: − 7 kJ·mol^{-1}, V–Ni: −18 kJ·mol^{-1}, and V–Mn: −1 kJ·mol^{-1}). Part of V atoms were incorporated with other elements to form the FCC phase when the V element is introduced into the CoFeNiMn HEAs. In contrast, remnant V atoms formed solid solution with other constituent elements, resulting in σ phase formation. The transformation from FCC phase to σ phase occurred as the V content increased. This caused the microstructure evolution in the CoFeNiMnV$_x$ HEAs.

The δ value decreased from 3.53 to 3.36% as the V content increased. The V addition minimized the atomic size difference, thus promoting the σ phase formation by destabilizing the FCC phase. Tsai et al. (Ref 31) proposed a modified VEC, which suggested that the σ phase formed when $6.88 \leq VEC \leq 7.84$. Figure 3 shows the plots of VEC and $\Delta\chi_A$ as a function of V content for the CoFeNiMnV$_x$ HEAs. Figure 4(a) shows that the calculated VEC in the CoFeNiMnV$_x$ HEAs decreased from 8.29 to 7.55. The modified VEC criterion is reliable to predict the σ phase formation. Figure 4(b) shows that the $\Delta\chi_A$ decreased steadily with an increase in V content. Thus, the reduction in both VEC and $\Delta\chi_A$ effectively promoted the formation of σ phase.

Table 1 Nominal composition and EDS analyses of the different regions in the CoFeNiMnV$_x$ HEAs. (at.%)

Alloys	Region	Co	Fe	Ni	Mn	V
V$_{0.25}$	Nominal	23.53	23.53	23.53	23.53	5.88
	FCC phase	24.94	24.38	22.40	21.72	6.56
	(Mn, Ni)-rich phase	16.16	14.28	26.66	38.70	4.20
V$_{0.50}$	Nominal	22.22	22.22	22.22	22.22	11.12
	FCC phase	23.77	23.55	21.22	19.31	12.15
	(Mn, Ni)-rich phase	19.43	19.37	21.42	28.15	11.63
V$_{0.75}$	Nominal	21.05	21.05	21.06	21.05	15.79
	FCC phase	21.16	19.56	20.91	21.86	16.51
	(Mn, Ni)-rich phase	17.64	18.25	18.65	27.91	17.55
V$_{1.00}$	Nominal	20	20	20	20	20
	FCC phase	19.52	18.20	18.52	21.46	22.30
	(Mn, Ni)-rich phase	16.42	17.59	16.13	24.68	25.18
V$_{1.25}$	Nominal	19.05	19.05	19.04	19.05	23.81
	FCC phase	19.28	17.44	21.31	19.35	22.62
	(Mn, Ni)-rich phase	18.26	17.84	18.20	19.95	25.75
	σ phase	18.67	18.31	15.54	19.31	28.17
V$_{1.50}$	Nominal	18.18	18.18	18.18	18.18	27.28
	FCC phase	18.00	16.36	19.22	19.16	27.26
	(Mn, Ni)-rich phase	17.77	17.28	18.48	19.34	27.13
	σ phase	18.76	17.38	16.17	19.37	28.32

The above analysis can provide theoretical guidance on the phase formation of the studied alloys. A steady decrease in δ with increased V content in the CoFeNiMnV$_x$ HEAs should promote the intermetallic σ phase formation by destabilizing the FCC solid-solution phase. In addition, the decrease in $\Delta\chi_A$ with increasing V content promotes σ phase formation based on previous reports (Ref 18, 22). Although VEC is larger than 8.0 in CoCrCuFeNiV HEAs (Ref 22), decreased VEC is critical in promoting the σ phase formation. Yang et al. (Ref 28) proposed that the solid-solution phase forms when $\Omega \geq 1.1$ and $\delta \leq 6.6\%$. Thus, a solid-solution phase should be formed for the CoFeNiMnV$_x$ HEAs in our study based on this criterion. The values of Ω and δ are within the solid-solution phase formation range. Alternatively, the values of Ω and δ are not beneficial in promoting the intermetallic phase formation. The σ phase formation in V–containing alloys is rather complex, and further studies are required to predict this phenomenon accurately.

3.4 Compression Properties and Microhardness

Compression tests were conducted on the CoFeNiMnV$_x$ HEAs. Figure 4 shows the compression stress–strain curves of the CoFeNiMnV$_x$ HEAs, and Table 5 summarizes the compressive properties such as yield strength ($\sigma_{0.2}$), fracture strength (σ_f), and fracture strain (ε_f). The results demonstrate that V addition remarkably impacted the compressive properties of the alloys. The alloys with $x \leq 1.00$ exhibited relatively low yield strength and an obvious work hardening stage after yielding. During the compression test, they did not fracture and exhibited excellent ductility with fracture strains larger than 55%. The $\sigma_{0.2}$ increased steadily from 223 to 355 MPa as V content increased from 0.25 to 1.00. Increasing V content significantly improved the strength of the alloys, whereas their ductility deteriorated. The yield strength increased sharply to 985 MPa for alloys with $x = 1.25$. Meanwhile, the V$_{1.25}$ alloys reached a high fracture strength of 1545 MPa with excellent plastic ductility ($\varepsilon_f = 26\%$). The strength of the alloys increased as the V content increased to $x = 1.50$; however, the ductility decreased. The V$_{1.50}$ alloys exhibited a maximum fracture strength of 1678 MPa and limited plastic ductility ($\varepsilon_f = 9.5\%$). Figure 5 shows the variation of Vickers microhardness as a

Table 3 Enthalpies of mixing between the major constituent elements (Unit: kJ·mol^{-1})

	Co	Fe	Ni	Mn	V
Co	…	− 1	0	− 5	− 14
Fe	− 1	…	− 2	0	− 7
Ni	0	− 2	…	− 8	− 18
Mn	− 5	0	− 8	…	− 1
V	− 14	− 7	− 18	− 1	…

Table 2 Physical parameters of the main constituent elements for the CoFeNiMnV$_x$ HEAs

Element	VEC	Atomic radius, nm	Melting point, K	Outer electron configurations	Electronegativity (Pauling)	Electronegativity (Allen)
Co	9	0.12510	1768	$3d^74s^2$	1.88	1.84
Fe	8	0.12412	1811	$3d^64s^2$	1.83	1.80
Ni	10	0.12459	1728	$3d^84s^2$	1.91	1.88
Mn	7	0.13500	1519	$3d^54s^2$	1.55	1.75
V	5	0.13160	2183	$3d^34s^2$	1.63	1.53

Table 4 Calculated values of valence electron concentration (VEC), enthalpy of mixing (ΔH_{mix}), mixing entropy (ΔS_{mix}), parameter Ω, atomic size difference (δ), and Allen electronegativity ($\Delta\chi_A$) of the CoFeNiMnV$_x$ HEAs

Alloys	VEC	ΔH_{mix}, kJ mol^{-1}	ΔS_{mix}, J mol^{-1} K^{-1}	Ω	δ, %	$\Delta\chi_A$, %
$V_{0.25}$	8.29	− 5.76	12.71	3.83	3.53	2.60
$V_{0.50}$	8.11	− 7.11	13.15	3.25	3.51	2.57
$V_{0.75}$	7.95	− 8.16	13.33	2.91	3.47	2.55
$V_{1.00}$	7.80	− 8.96	13.38	2.69	3.44	2.52
$V_{1.25}$	7.67	− 9.58	13.34	2.54	3.40	2.50
$V_{1.50}$	7.55	− 10.05	13.25	2.42	3.36	2.48

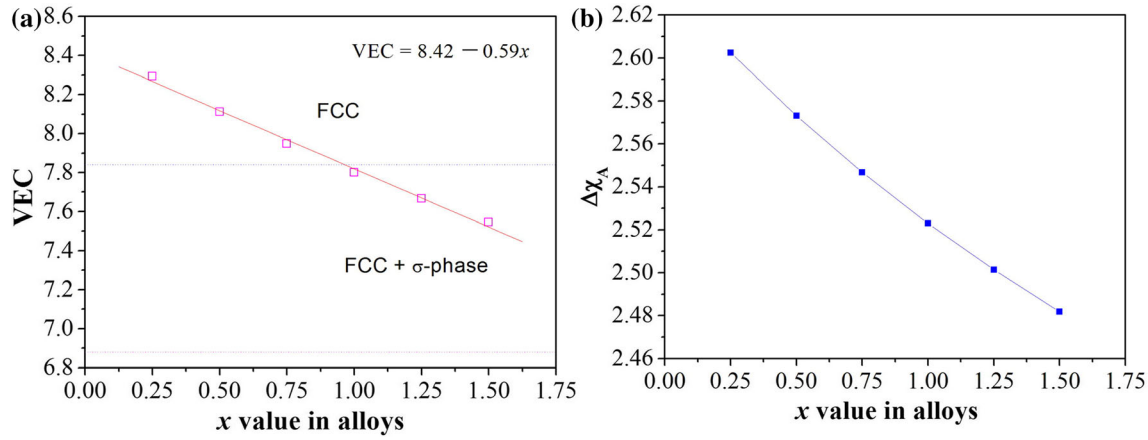

Fig. 3 Variation of VEC and $\Delta\chi_A$ as a function of V content in the CoFeNiMnV$_x$ HEAs (a, b)

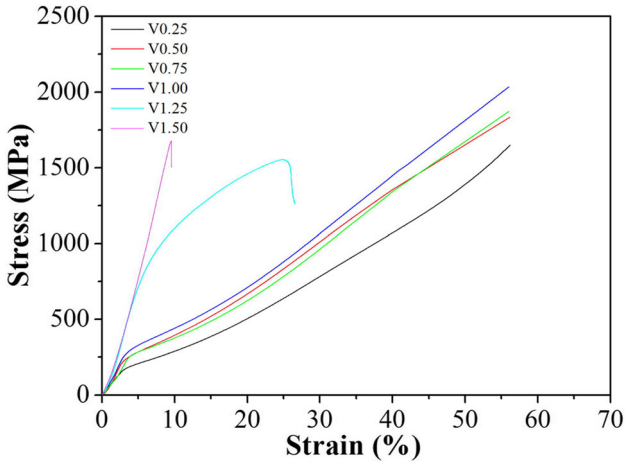

Fig. 4 Stress–strain curves obtained during compressive tests of the CoFeNiMnV$_x$ HEAs

function of V content obtained from the CoFeNiMnV$_x$ HEAs. The alloys with x = 0.25 exhibited a 213-HV microhardness. A further increase in the V content significantly affected their microhardness, which increased from 213 HV for alloys with x = 0.25 to 716 HV for alloys with x = 1.50. The results demonstrated the Vickers microhardness dependence on the V content. In addition, the Vickers microhardness of the alloys significantly increased with an increase in the fraction of the precipitated σ phase. The increase in strength and hardness with

Table 5 Compression yield strength ($\sigma_{0.2}$), fracture strength (σ_f), and fracture strain (ε_f) of the CoFeNiMnV$_x$ HEAs

Alloys	$\sigma_{0.2}$, MPa	σ_f, MPa	ε_f .%
$V_{0.25}$	223	No fracture	> 55
$V_{0.50}$	306	No fracture	> 55
$V_{0.75}$	315	No fracture	> 55
$V_{1.00}$	355	No fracture	> 55
$V_{1.25}$	985	1545	26
$V_{1.50}$	1545	1678	9.5

an increase in V content is attributable to the solid solution and precipitation strengthening caused by the σ phase formation.

The FCC phase exhibits low strength and excellent plasticity, whereas the σ phase exhibits high strength and limited plasticity. According to the simple rule of mixtures (Ref 32, 33), the yield strength of the alloys, $\sigma_{0.2}$, can be expressed as follows:

$$\sigma_{0.2} = V_{FCC}\sigma_{FCC} + V_{BCC}\sigma_{BCC} \quad \text{(Eq 7)}$$

where σ_{FCC} and $\sigma_{\sigma\ phase}$ represent the strength of the FCC and σ phase, respectively; V_{FCC} and V_σ are the volume fraction of the FCC and σ phase, respectively.

Equation 7 describes the strength enhancement of the HEAs due to σ phase strengthening. The yield strength of the alloys could be significantly enhanced with an increased volume fraction in the σ phase. For the σ-phase-containing CoFe-

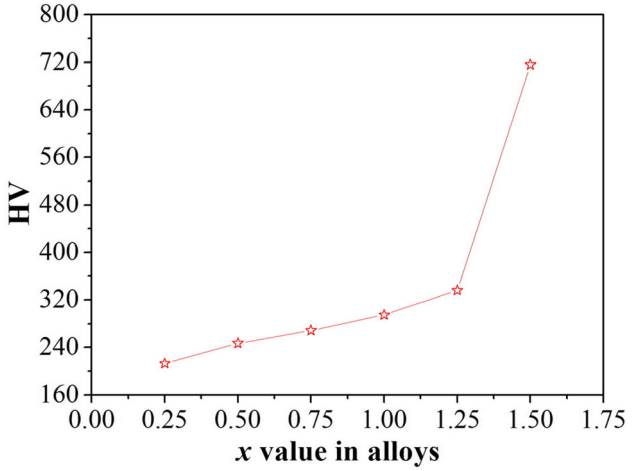

Fig. 5 Relationship between Vickers microhardness and V content of the $CoFeNiMnV_x$ HEAs

$NiMnV_x$ HEAs, increasing V content results in an increased volume fraction of σ phase and refined grain size. They are expected to be effective obstacles for hindering the dislocation movement along with the FCC matrix, thus producing a strengthening effect. Further, a ductile to brittle fracture transition occurred as the volume fraction of σ phase increased. The ductility of the $CoFeNiMnV_x$ HEAs exhibits nonmonotonical dependence with the σ phase volume fraction. The ductility decreases even further when the σ phase becomes the matrix phase (Ref 17).

4. Conclusion

In this study, the alloying effect of V addition on the phase formation, microstructure, and mechanical properties of $CoFeNiMnV_x$ HEAs is investigated, and the following conclusions are drawn.

(1) V addition promotes phase transition from the FCC phase to the σ phase by destabilizing the FCC phase. The precipitation of σ phase is directly associated with the V content in alloys. Only a single-phase FCC solid-solution structure is observed for alloys with $x \leq 1.00$, whereas a coexistence of FCC and σ phases is visible for alloys with $x > 1.00$. EDS analysis indicates that the σ phase in the $CoFeNiMnV_x$ HEAs is significantly enriched with V, and the atomic concentration of V within the σ phase is up to 28%.

(2) Typical dendritic structures are observed in the $CoFeNiMnV_x$ alloys. The dendrite regions are slightly enriched with Co, Fe, and V, whereas the interdendritic regions are enriched with Mn and Ni. XRD and microstructural analysis indicate that the formation of σ phase occurs in the microstructure of alloys with $x > 1.00$.

(3) The decreased VEC and $\Delta\chi_A$ promote the formation of σ phase in the microstructure.

(4) V addition in the CoFeNiMn alloy results in continuous strengthening without an increase in ductility. Alloys with $x \leq 1.00$ exhibit excellent ductility with a steady increase in yield strength from 223 to 355 MPa. However, a further increase in V content ($x > 1.00$) remarkably increases the strength and decreases the ductility of the alloys. The microhardness first increases steadily from 213 HV for $V_{0.25}$ alloys to 336 HV for $V_{1.25}$ alloys and then increases sharply to 716 HV for $V_{1.50}$ alloys.

Acknowledgments

This research work was funded by the National Natural Science Foundation of China (Nos. 51301125, 51971166, 51904218), the Natural Science Foundation of Shaanxi Province (No. 2020JM-557), and the State Key Laboratory of Solidification Processing in NWPU (No. SKLSP201811).

References

1. J.W. Yeh, S.K. Chen, S.J. Lin, J.Y. Gan, T.S. Chin, T.T. Shun, C.H. Tsau and S.Y. Chang, Nanostructured High-Entropy Alloys with Multiple Principal Elements: Novel Alloy Design Concepts and Outcomes, *Adv. Eng. Mater.*, 2004, **6**, p 299–303
2. J.W. Yeh, S.Y. Chang, Y.D. Hong, S.K. Chen and S.J. Lin, Anomalous Decrease in X-ray Diffraction Intensities of Cu–Ni–Al–Co–Cr–Fe–Si Alloy Systems with Multi-Principal Elements, *Mater. Chem. Phys.*, 2007, **103**, p 41–46
3. Y.P. Lu, Y. Dong, S. Guo, L. Jiang, H.J. Kang, T.M. Wang, B. Wen, Z.J. Wang, J.C. Jie, Z.Q. Cao, H.H. Ruan and T.J. Li, A Promising New Class of High-Temperature Alloys: Eutectic High-Entropy Alloys, *Sci. Rep.*, 2014, **4**, p 6200
4. K.X. Zhou, J.J. Li, Q.F. Wu, Z.L. Zhang, Z.J. Wang and J.C. Wang, Remelting Induced Fully-Equiaxed Microstructures with Anomalous Eutectics in the Additive Manufactured $Ni_{32}Co_{30}Cr_{10}Fe_{10}Al_{18}$ Eutectic High-Entropy Alloy, *Scripta Mater.*, 2021, **201**, p 113952
5. N. Liu, W. Ding, X.J. Wang, J. Zhang, P.J. Zhou and C. Mu, Phases, Microstructures and Properties of Multi-Component FeCoNi-Based Alloys, *Mater. Sci. Technol.*, 2020, **36**, p 654–660
6. N. Liu, M. Xu, Y.Y. Qian and P.J. Zhou, Microstructure, Phase Stability, and Oxidation Resistance of $(FeCoNi)_{60}Al_{15}Cr_{25-x}Ti_x$ High-Entropy Alloys, *J. Alloys. Compd.*, 2021, **870**, p 159320
7. A. Verma, P. Tarate, A.C. Abhyankar, M.R. Mohape, D.S. Gowtam, V.P. Deshmukh and T. Shanmugasundaram, High Temperature Wear in $CoCrFeNiCu_x$ High Entropy Alloys: The Role of Cu, *Scripta Mater.*, 2019, **161**, p 28–31
8. H. Jiang, D.X. Qiao, Y.P. Lu, Z. Ren, Z.Q. Cao, T.M. Wang and T.J. Li, Direct Solidification of Bulk Ultrafine-Microstructure Eutectic High-Entropy Alloys with Outstanding Thermal Stability, *Scripta Mater.*, 2019, **165**, p 145–149
9. Y. Yu, F. He, Z.H. Qiao, Z.J. Wang, W.M. Liu and J. Yang, Effects of Temperature and Microstructure on the Triblogical Properties of CoCrFeNiNbx Eutectic High Entropy Alloys, *J. Alloys Compd.*, 2019, **775**, p 1376–1385
10. Z.J. Wang, Y.Y. Huang, Y. Yang, J.C. Wang and C.T. Liu, Atomic-size Effect and Solid Solubility of Multicomponent Alloys, *Scripta Mater.*, 2015, **94**, p 28–31
11. C.B. Wei, L.W. Li, Y.P. Lu, X.H. Du and T.M. Wang, Evolution of Microstructure and Mechanical Properties of As-Cast $AlxCrFe_2N_2$ High-Entropy Alloys with Al Content, *Metall. Mater. Trans. A*, 2021, **52**, p 1850–1860
12. Y.P. Lu, X.Z. Gao, L. Jiang, Z.N. Chen, T.M. Wang, J.C. Jie, H.J. Kang, Y.B. Zhang, S. Guo, H.H. Ruan, Y.H. Zhao, Z.Q. Cao and T.J. Li, Directly Cast Bulk Eutectic and Near-Eutectic High Entropy Alloys with Balanced Strength and Ductility in a Wide Temperature Range, *Acta Mater.*, 2017, **124**, p 143–150
13. T.X. Li, Y.P. Lu, T.M. Wang and T.J. Li, Grouping Strategy via d-orbit Energy Level to Design Eutectic High-Entropy Alloys, *Appl. Phys. Lett.*, 2021, **119**, p 071905

14. M.N. Zhang, X.L. Zhou and J.H. Li, Microstructure and Mechanical Properties of a Refractory CoCrMoNbTi High-Entropy Alloy, *J. Mater. Eng. Perform.*, 2017, **26**, p 3657–3665
15. L.P. Huang, M.H. Long, W.S. Liu and S. Li, Effects of Cr on Microstructure, Mechanical Properties and Hydrogen Desorption Behaviors of ZrTiNbMoCr High Entropy Alloys, *Mater. Lett.*, 2021, **293**, p 129718
16. X.J. Wang, M. Xu, N. Liu and L.X. Liu, The Formation of Sigma Phase in the CoCrFeNi High-Entropy Alloys, *Mater. Res. Express*, 2021, **8**, p 076514
17. G.A. Salishchev, M.A. Tikhonovsky, D.G. Shaysultanov, A.V. Kuznetsov, I.V. Kolodiy, A.S. Tortika and O.N. Senkov, Effect of Mn and V on Structure and Mechanical Properties of High-Entropy Alloys Based on CoCrFeNi System, *J. Alloys Compd.*, 2014, **591**, p 11–21
18. N.D. Stepanov, D.G. Shaysultanov, G.A. Salishchev, M.A. Tikhonovsky, E.E. Oleynik, A.S. Tortika and O.N. Senkov, Effect of V Content on Microstructure and Mechanical Properties of the CoCrFeMnNiV_x High Entropy Alloys, *J. Alloys Compd.*, 2015, **628**, p 170–185
19. G. Qin, Z.B. Li, R.R. Chen, H.T. Zheng, C.L. Fan, L. Wang, Y.Q. Su, H.S. Ding, J.J. Guo and H.Z. Fu, CoCrFeMnNi High-Entropy Alloys Reinforced with Laves Phase by Adding Nb and Ti Elements, *J. Mater. Res.*, 2019, **34**, p 1011–1020
20. M.R. Chen, S.J. Lin, J.W. Yeh, M.H. Chuang, S.K. Chen and Y.S. Huang, Effect of Vanadium Addition on the Microstructure, Hardness, and Wear Resistance of $Al_{0.5}$CoCrCuFeNi High-Entropy Alloy, *Metall. Mater. Trans. A*, 2006, **37**, p 1363–1369
21. N.Y. Yurchenko, N.D. Stepanov, D.G. Shaysultanov, M.A. Tikhonovsky and G.A. Salishcheva, Effect of Al Content on Structure and Mechanical Properties of the Al_xCrNbTiVZr (x = 0; 0.25; 0.5; 1) High-Entropy Alloys, *Mater. Charac.*, 2016, **121**, p 125–134
22. T.T. Zuo, Microstructure and Properties of Co-Fe-Ni Based Magnetic High Entropy Alloys, Ph.D. Thesis, University of Science and Technology Beijing, 2016
23. G. Qin, S. Wang, R.R. Chen, H.T. Zheng, L. Wang, Y.Q. Su, J.J. Guo and H.Z. Fu, Improvement of Microstructure and Mechanical Properties of CoCrCuFeNi High-Entropy Alloys by V Addition, *J. Mater. Eng. Perform.*, 2019, **28**, p 1049–1056
24. R.R. Chen, G. Qin, H.T. Zheng, L. Wang, Y.Q. Su, Y.L. Chiu, H.S. Ding, J.J. Guo and H.Z. Fu, Composition Design of High Entropy Alloys Using the Valence Electron Concentration to Balance Strength and Ductility, *Acta Mater.*, 2018, **144**, p 129–137
25. Y. Zhang, Y.J. Zhou, J.P. Lin, G.L. Chen and P.K. Liaw, Solid-solution Phase Formation Rules for Multi-Component Alloys, *Adv. Eng. Mater.*, 2008, **10**, p 534–538
26. S. Guo, C. Ng, J. Lu and C.T. Lu, Effect of valence Electron Concentration on Stability of fcc or bcc Phase in High Entropy Alloys, *J. Appl. Phys.*, 2011, **109**, p 103505
27. S. Guo and C.T. Liu, Phase Stability in High Entropy Alloys: Formation of Solid-Solution Phase or Amorphous Phase, *Prog. Nat. Sci.: Mater*, *Int.*, 2011, **21**, p 433–446
28. X. Yang and Y. Zhang, Prediction of High-Entropy Stabilized Solid-Solution in Multicomponent Alloys, *Mater. Chem. Phys.*, 2012, **132**, p 233–238
29. B. Chanda and J. Das, Composition Dependence on the Evolution of Nanoeutectic in CoCrFeNiNbx ($0.45 \leq x \leq 0.65$) High Entropy Alloys, *Adv. Eng. Mater.*, 2018, **20**, p 1700908
30. F.R. de Boer, R. Boom, W.C.M. Mattens, A.R. Miedema, and A.K. Niessen Eds., *Cohesion in Metals: Transition Metal Alloys*, North Holland Physics, Amsterdam, 1988
31. M.H. Tsai, K.Y. Tsai, C.W. Tsai, C. Lee, C.C. Juan and J.W. Yeh, Criterion for Sigma Phase Formation in Cr- and V-Containing High-Entropy Alloys, *Mater. Res. Lett.*, 2013, **1**, p 207–212
32. K.U. Kainer, Metal Matrix Composites, Betz-Druck GmbH, Darmstadt, 2006
33. W.Y. Huo, H. Zhou, F. Fang, X.F. Zhou, Z.H. Xie and J.Q. Jiang, Microstructure and Properties of Novel CoCrFeNiTa$_x$ Eutectic High-Entropy Alloys, *J. Alloys Compd.*, 2018, **735**, p 897–904